Paper published as

Tancredi,U., Renga,A., and Grassi M. Real-Time Relative Positioning of Spacecraft over Long Baselines. Journal of Guidance, Control, and Dynamics 2014 37:1, 47-58

http://arc.aiaa.org | DOI: 10.2514/1.61950

Real-time relative positioning of spacecraft over long baselines

Urbano Tancredi[1]
University of Naples Parthenope, Napoli, 80143, Italy

and
Alfredo Renga[2], Michele Grassi[3]
University of Naples Federico II, Napoli, 80125, Italy

This paper deals with the problem of real-time onboard relative positioning of low Earth orbit spacecraft over long baselines using the Global Positioning System. Large inter-satellite separations, up to hundreds of kilometers, are of interest to multistatic and bistatic Synthetic Aperture Radar applications, in which highly accurate relative positioning may be required in spite of the long baseline. To compute the baseline with high accuracy the integer nature of dual-frequency, double-difference carrier-phase ambiguities can be exploited. However, the large inter-satellite separation complicates the integer ambiguities determination task due to the presence of significant differential ionospheric delays and broadcast ephemeris errors. To overcome this problem, an original approach is proposed, combining an extended Kalman filter with an integer least square estimator in a closed-loop scheme, capable of fast on-the-fly integer ambiguities resolution. These integer solutions are then used to compute the relative positions with a single-epoch kinematic least square algorithm that processes ionospheric-free combinations of de-biased carrier-phase measurements. Approach performance and robustness are assessed by using the flight data of the Gravity Recovery and Climate Experiment mission. Results show that the baseline can be computed in real-time with decimeter-level accuracy in different operating conditions.

---

[1] Assistant Professor, Department for Technologies, Centro Direzionale C4, AIAA Member.
[2] Contract Researcher, Department of Industrial Engineering, Piazzale Tecchio 80.
[3] Professor, Department of Industrial Engineering, Piazzale Tecchio 80, AIAA Member.

I. Introduction

Space applications like spaceborne remote sensing, geodesy, multidimensional magnetosphere investigation, and universe observation by space interferometry require simultaneous observations taken at largely separated points in space, preventing the use of a single monolithic platform. With specific reference to Low Earth Orbit (LEO) missions, remote sensing applications based on using Synthetic Aperture Radars (SAR) are meaningful examples of formation flying. Cross-Track Interferometry (XTI) and Large-Baseline Bistatic (LBB) SAR applications rely on processing radar images of the same scene produced by two or more physically separated antennas [1]–[3], which shall be distributed on different spacecraft following specific relative orbital paths in order to realize the desired separation. The size of the physical separation, i.e. the baseline, depends on the considered application, and can range from a few hundreds of meters in XTI applications [1],[2] to a few hundreds of kilometers in LBB SAR missions [3]. Depending on the application, the knowledge of the inter-satellite separation up to the millimeter level may be required also over very long baselines (i.e. hundreds of kilometers). Even though this accuracy is needed on ground and not in real-time for scientific data processing [4], the capability of determining the baseline on board with an accuracy in the order of a decimeter can be of potential interest for future distributed Earth observation systems based on flying multiple low-cost small platforms. Formation management and scientific applications can greatly benefit from an increased autonomy level [5], performing operations as formation control and image generation on board thanks to a precise knowledge of the baseline.

Carrier-phase Differential GPS (CDGPS) is a promising solution to have highly precise relative position fixes. Its capability to achieve accurate relative positions, i.e. at the cm-level or even better, is essentially based on the possibility to exploit the integer nature of Double Difference (DD) carrier-phase ambiguities. Several previous studies have investigated its performance in LEO formations, especially for short separations (up to tens of kilometers) [6]-[9]. As the separation among the satellites increases, the correlation of ionospheric delays [9] and broadcast ephemeris errors [10] among the receivers decreases. DD GPS observables are thus affected by significant errors that, if not properly considered, complicate the integer resolution task, spoiling the stability of the relative navigation solution, which can easily diverge. Relatively few works have dealt with long-baseline applications [10]–[12], exploiting dual frequency measurements and final (ephemeris) products. Dual-frequency GPS receivers allow observing and, then, compensating ionospheric path delays, and ephemeris errors can be drastically reduced by using final products instead of ephemeris data broadcast along with the ranging signal. In addition, residual differential errors are filtered out in

these applications with dynamic filters relying on complex, high-fidelity absolute and relative dynamics models. Experimentations on true-world GPS flight data demonstrated the capability for mm-scale relative positioning [11] of this approach, if complemented by smoothing techniques in which filter results are processed backward and forward. However, precise ephemeris are not available on board, and smoothing techniques cannot be used in real-time applications. Moreover, the use of high-complexity dynamic models is limited in onboard implementations by the significant computational load [13].

Compared to the above dynamic-based schemes, kinematic-based approaches show some interesting features for onboard implementation. The computational load is notably smaller and results are not affected by the inaccuracies of the considered dynamics models, so kinematic approaches can be used also during satellite maneuvers. The main drawback is the reduced observability of the unknowns, since the time correlation introduced by dynamics models cannot be exploited. This can also cause a temporary loss of the solution due to an unfavorable observation geometry or an insufficient number of GPS satellites. Purely kinematic approaches have been rarely proposed for long baseline formations [14],[15]. Of these, only one exploits the integer nature of DD carrier-phase ambiguities [15].

Conversely, Real-Time Kinematic (RTK) schemes implemented in the present generation dual-frequency GPS receivers for long baseline terrestrial applications are a mature technology. Autonomous relative positioning between ground-based receivers is routinely performed with accuracies in the order of few centimeters for horizontal baselines, whereas larger separations require long initialization times and multi-baseline network solutions [16],[17]. The core of terrestrial RTK schemes is the capability to produce fast, accurate, and robust solutions for carrier-phase integer ambiguities. These solutions are then used to remove the contribution of the integer ambiguities from the ionospheric-free combination [18] of dual-frequency carrier-phase observables. The resulting de-biased carrier-phase measurements yield the final accurate baseline estimation typically computed by kinematic least-squares algorithms [16] – [18].

The same approach can be extended to satellite relative positioning. With respect to terrestrial applications, RTK can take advantage of the rapidly changing Line-of-Sight (LoS) vector to GPS satellites, which can speed up the ambiguity resolution [15], and of the smaller magnitude of atmospheric effects at LEO altitudes. Even though these advantages might enable successful kinematic relative positioning over baselines longer than for ground-based applications, there are important practical limitations for the satellite case. The GPS observation geometry is in general worse than in the terrestrial case due to the receiver's altitude. Furthermore, fast dynamics make ambiguities

observable but, at the same time, the number of the tracked GPS satellites is much more variable. Hence, simple accumulation of integer ambiguity estimates over several time epochs [15] is not a successful strategy for reliable, on the fly, ambiguity resolution. The approach pursued herein is to include simple dynamical models that increase the ambiguities' observability by providing time correlation to the other unknowns, most notably the geometric term.

More precisely, this paper presents an original dual frequency, CDGPS-based, filtering approach specifically designed for precise real-time relative positioning of long baseline LEO formations, and for possible onboard application. It extends the RTK technique to spaceborne applications, by separating the computation of the integer ambiguities from the relative positioning solution, as in previous terrestrial [16], [17], and satellite [15] RTK approaches. The main novelty of the proposed approach is the development of a new closed-loop dynamic filter scheme to perform reliable and robust on-the-fly ambiguity resolution. This closed-loop scheme fully integrates the dynamic filter with an integer resolution step to exploit the integer nature of DD ambiguities for improving the dynamic filter's solution.

The proposed approach consists in a two-step solution. The first step estimates DD integer ambiguities using as little computational effort as possible. More specifically, DD Wide Lane (WL) and L1 Integer Ambiguities (IA) are computed as the solution of a closed-loop dynamic filter that combines an Extended Kalman Filter (EKF) with a standard Integer Least Square (ILS) estimator. To support the integer ambiguities resolution, DD ionospheric delays terms are specifically modeled in the filter by means of the Vertical Total Electron Content (VTEC). In contrast to the previous approaches, the closed-loop dynamic filter exploits a simple non-linear model of the relative dynamics. This, together with specifically designed integer validation procedures, provides an accuracy adequate to solve the integer ambiguities while preventing filter instability and reducing the computational effort to a level suitable for onboard implementation. Assuming that a set of integer ambiguities is correctly resolved, and therefore perfectly known, the second step provides the relative position with high accuracy. To this end, it employs only ionosphere-free combinations of carrier phase measurements de-biased with the fixed integer ambiguities. The relative position fix results from a single-epoch least-square kinematic filter, which requires very low additional computational resources.

The remainder of the paper is organized as follows. The concept of precise relative positioning over long baselines by CDGPS in real-time is reviewed in the next section. The techniques proposed for on-the-fly ambiguity resolution and for obtaining the single-epoch kinematic solution are discussed in detail in sections III and IV, respectively. At

last, performance of the developed filtering approach is assessed in section V using real flight data from the Gravity Recovery and Climate Experiment (GRACE) mission.

II. Long-baseline Real Time Relative Positioning by CDGPS

The present paper focuses on a formation of two LEO satellites (chief and deputy), separated by a distance in the order of hundreds of kilometers, having similar shapes and a three axis stabilized, nadir-pointing attitude, as typical in remote sensing applications. Spaceborne geodetic-grade dual frequency receivers, such as the one in [6], are considered as the primary navigation sensor. Relative positions are sought in real-time by an algorithm suitable for onboard implementation. It makes indeed a limited use of computational resources and exploits only data available on board, most notably broadcast ephemeris. However, onboard applications require solving a series of implementation challenges (e.g. time synchronization, telemetry between the satellites, in-flight calibration) which influence the accuracy achievable by the algorithm. The severity and mitigation of such effects heavily depends on the specific mission. Their detailed discussion is out of the scope of this work, which refers to a standard formation flying scenario, where the chief satellite is supposed to receive deputy GPS observables by means of a satellite inter-link and the positioning is performed on board the chief satellite. Observables will thus be affected by a latency that is expected to range from a few tenths of second to 1 second at most [14] depending on the specific mission, which is compatible with the time scale of the relative dynamics in long baseline LEO formations.

GPS measurements are assumed to be synchronized prior to be processed for relative positioning. The considered GPS receivers are characterized by the capability to align the receiver time to GPS time within a tolerance margin generally better than 1 μs. This is achieved by steering the internal oscillator based on the clock error of the receiver, obtained as part of the navigation solution [14],[19]. The raw GPS observables are thus aligned to integer seconds of the GPS time with an error smaller than 1 μs. Uncompensated timing residuals of this magnitude are treated as errors of the observation models, as discussed later on. The receivers on board the two satellites are therefore capable of delivering four GPS observables tagged at integer seconds of the GPS time t_k, one pseudorange and one carrier-phase measurement per each of the two L1 and L2 frequencies. The following standard model [18] is used to relate these observables to the observation geometry. Explicit time dependency is omitted for conciseness, in this case and whenever it can be clearly devised by the context.

$$\left(P_1\right)_{rec}^{sv} = \left\|\boldsymbol{\rho}_{rec}^{sv}\right\| + c\delta t_{rec} - c\delta t^{sv} + i_{rec}^{sv} + \left(\varepsilon_{P1}\right)_{rec}^{sv} \tag{1a}$$

$$\left(P_2\right)_{rec}^{sv} = \left\|\boldsymbol{\rho}_{rec}^{sv}\right\| + c\delta t_{rec} - c\delta t^{sv} + \gamma^{-2} i_{rec}^{sv} + \left(\varepsilon_{P2}\right)_{rec}^{sv} \tag{1b}$$

$$\left(L_1\right)_{rec}^{sv} = \left\|\boldsymbol{\rho}_{rec}^{sv}\right\| + c\delta t_{rec} - c\delta t^{sv} - i_{rec}^{sv} + \lambda_1 \psi_{1,rec}^{sv} + \left(\varepsilon_{L1}\right)_{rec}^{sv} \tag{1c}$$

$$\left(L_2\right)_{rec}^{sv} = \left\|\boldsymbol{\rho}_{rec}^{sv}\right\| + c\delta t_{rec} - c\delta t^{sv} - \gamma^{-2} i_{rec}^{sv} + \lambda_2 \psi_{2,rec}^{sv} + \left(\varepsilon_{L2}\right)_{rec}^{sv} \tag{1d}$$

In Eq.(1), *P* and *L* stand for the pseudorange and carrier phase measurements, respectively, expressed in meters, the subscripts 1 and 2 indicate the L1 and L2 frequency, and *sv* denotes the GPS Satellite Vehicle (SV) from which the measurement is taken by the receiver *rec*. The LoS distance between the SV *sv* and the receiver *rec* is denoted by $\left\|\boldsymbol{\rho}_{rec}^{sv}\right\|$, the receiver and SV clock biases by $c\cdot\delta t_{rec}$ and $c\cdot\delta t^{sv}$, respectively, *c* being the speed of light in vacuum. Because the receivers are above the troposphere and part of the ionosphere, the atmosphere induces only a dispersive delay due to the remaining ionosphere, which on the L1 frequency is denoted as i_{rec}^{sv}. Only first order ionospheric delays are accounted for, which depend on the inverse square of carrier frequency and have an anti-symmetric effect on pseudoranges and carrier-phase. The ionospheric delay on L2 is thus univocally determined by i_{rec}^{sv} and the ratio between GPS signal wavelengths, $\gamma=\lambda_1/\lambda_2$. The carrier phase equation on the frequency *f* includes also the cycle ambiguity term $\lambda_f \psi_{f,rec}^{sv}$. This term represents the difference between the initial values of the transmitted and internal receiver replica signal's phase, and is a real number that does not change until phase lock is lost between *sv* and *rec*. All other error terms, most notably multipath, line bias, measurement noise, and polarization induced windup for carrier-phase measurements [20], are enclosed into the ε term, which is thus assumed to depend on both the SV and the receiver and is typically different for L1 and L2 frequencies.

Eq.(1) depend on the receiver and SV absolute position vectors, $\mathbf{r}_{rec}$ and $\mathbf{R}^{sv}$, respectively, via the $\boldsymbol{\rho}_{rec}^{sv}$ vector. Note that for computing the LoS distance travelled by the ranging signals in Eq.(1), the SV position must be taken at the time at which the signal left the transmitter, that is, t_k minus the signal propagation time ϑ_{rec}^{sv}. Letting the subscripts *d* and *c* refer to the receivers on board the deputy and chief satellites, respectively, the LoS distance vectors read

$$\begin{aligned} \boldsymbol{\rho}_c^{sv}\left(t_k\right) &= \mathbf{R}^{sv}\left(t_k - \vartheta_c^{sv}\right) - \mathbf{r}_c\left(t_k\right) \\ \boldsymbol{\rho}_d^{sv}\left(t_k\right) &= \mathbf{R}^{sv}\left(t_k - \vartheta_d^{sv}\right) - \mathbf{r}_c\left(t_k\right) - \mathbf{b}\left(t_k\right) \end{aligned} \tag{2}$$

The application of ephemeris data yields uncertainties in the SV position and generates an effect that is similar to a miscalculation of the transmission time. The first order effect on the LoS distance depends on the projection of the

SV vector position error onto the LoS direction [18], which makes the ephemeris error dependent also upon the receiver position. When using broadcast ephemeris, this ranging error has a representative magnitude of few meters, which is the limiting factor for dual-frequency spaceborne GPS receivers [21]. The time tag accuracy of the considered GPS receivers also affects the computed LoS distance. This effect depends on the product of the time tag error and the projection of both SV and receiver velocity on the LoS direction and is sub-centimetric for the considered GPS receivers in LEO.

Starting from the observation model of Eq.(1), observations of the same kind, e.g. P_1, can be differenced for deleting the common-mode errors that affect the receivers' absolute positions to the same extent, and thus do not impact their relative position. More specifically, Single Difference (SD) observations are obtained by taking the difference of measurements from the same SV *j* between two receivers. This allows deleting all SV-generated common mode errors, such as the SV clock bias. The difference between all receiver-generated common-mode errors, including the clock biases explicitly mentioned in Eq.(1) and other effects such as line delays, still appears in SD observables. However, it can be cancelled by forming DD observables, i.e. differencing SD observations between a GPS satellite *j*, denoted as the pivot, and any other SV *k* in view of both receivers. Only the terms jointly depending on the SV and the receiver do not cancel, such as the DD geometric term, which combines the four relevant LoS ranges shown in Fig. 1 as $g^{jk} = \left\|\boldsymbol{\rho}_d^k\right\| - \left\|\boldsymbol{\rho}_d^j\right\| - \left\|\boldsymbol{\rho}_c^k\right\| + \left\|\boldsymbol{\rho}_c^j\right\|$. Depending on the unknown position vectors of both receivers, this term is customarily manipulated for determining the relative position **b** of the deputy receiver w.r.t. the chief one, using an independently determined estimate of the chief position $\mathbf{r}_c$, e.g. obtained by Eq.(1). The DD geometric term can be related to the DD observables by the following standard model, shown only on the L1 frequency for compactness.

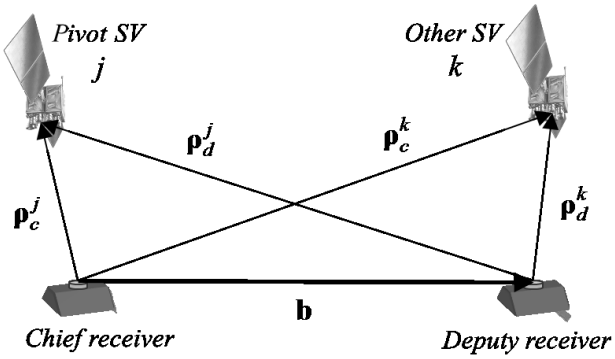

Fig. 1 Double differencing for relative positioning.

$$P_1^{jk} = g^{jk} + i^{jk} + \varepsilon_{P1}^{jk} \tag{3a}$$

$$L_1^{jk} = g^{jk} - i^{jk} + \lambda_1 n_1^{jk} + \varepsilon_{L1}^{jk} \tag{3b}$$

DD terms are denoted by the same symbol of non-differenced ones, but with no receiver subscript and double SV indexes as superscript, with the exception of the cycle ambiguity term $n_1^{jk} = \psi_{1,d}^{k} - \psi_{1,d}^{j} - \psi_{1,c}^{k} + \psi_{1,c}^{j}$, expressed in cycles. DD broadcast ephemeris errors induce a systematic error on both pseudorange and carrier-phase observables by means of the geometric term g^{jk}. The non-common aliquot of the ephemeris error is due to the misalignment of LoS unit vectors pointing to the same SV, which increases with the baseline magnitude, but it is not modeled explicitly in Eq.(3). The effect of the time tag errors, which are different for the two GPS receivers, is an additional error to the DD geometric term. However, its magnitude does not strictly depend on the baseline but it is dominated by the projection onto the LoS vectors of the vector sum of the velocities of the receivers [22]. The worst case is therefore when the velocities of the receivers are aligned, which is always very likely in LEO formation flying for remote sensing, when the orbits are almost parallel. The amount of this error is however not expected to exceed 1-2 cm when the time tag error is lower than 1 μs, as for geodetic-grade GPS receivers. Other residual, non-common-mode, systematic errors, like polarization induced windup, antenna phase-center variations, and multipath, are enclosed in the noise term ε as they tend to be smaller than the ephemeris error.

The ionospheric delay is also reduced by the differencing operations. The magnitude of this term depends on the baseline between the two receivers and on the ionosphere electron content. For typical solar conditions, this term is negligible for baselines under about 10 km [11], whereas it can be in the order of the meter for baselines of few hundreds of kilometers [23]. Dual frequency measurements are essential for compensating such term, as DD carrier-phase measurements can be used to form the following ionospheric-free observable.

$$\frac{1}{1-\gamma^2}\left(L_1^{jk} - \gamma^2 L_2^{jk}\right) = g^{jk} + \frac{\lambda_1}{1-\gamma^2}\left(n_1^{jk} - \gamma n_2^{jk}\right) + \varepsilon_{LIF}^{jk} \tag{4}$$

CDGPS techniques over long baselines take advantage of Eq.(4) for achieving a highly accurate relative position. As thoroughly discussed in [20], to which the interested reader is referred, the cycle ambiguity n_f^{jk} becomes integer after double differencing, provided that the receivers are properly designed. Knowledge of the integer nature of the ambiguities allows compensating exactly the cycle ambiguity term in Eq.(4), at least in principle. In some cases, including this paper, the wide-lane (WL) combination [18] of L1 and L2 ambiguities, $n_w = n_1 - n_2$, is used in place of

L2 ambiguities. Despite the chosen ambiguity parameterization, two independent integer ambiguity estimates are needed for de-biasing the observables in Eq.(4). These de-biased ionospheric-free DD carrier-phase observables allow directly sampling the DD geometric term with an accuracy comparable to the sub-centimetric carrier-phase measurement noise, provided that systematic errors in the ε_{LIF} term are negligible. This feature is the key element used by RTK techniques for precise relative positioning over long baselines.

The DD observables have some distinctive features. Double differencing reduces by one the number of each GPS observable, because the pivot SV measurements are used in all DD observables, which also introduces a correlation between different DD measurements. GPS non-differenced observables are instead customarily modeled as mutually uncorrelated, each one affected by the relevant ε term that is assumed a Gaussian zero-mean noise. Letting p+1 be the number of SV simultaneously tracked by both receivers and denoting generically with X_f both pseudoranges and carrier-phase observables on the frequency f, the non-differenced observables in view of the receiver *rec,* $\left(\mathbf{X}_f\right)_{rec} = \left(X^1_{rec} \quad ... \quad X^p_{rec} \quad X^j_{rec}\right)^T$, have a diagonal covariance matrix with equal variances σ^2_{Xf}. Double differencing combines the observables of both receivers applying the following linear transformation

$$\mathbf{X}^j_f = T_{DD}\begin{bmatrix}\left(\mathbf{X}_f\right)_d \\ \left(\mathbf{X}_f\right)_c\end{bmatrix} \tag{5a}$$

$$T_{DD} \in \mathbb{R} \qquad , \; T_{DD} = \left(I_p \quad -U_{p,1} \quad -I_p \quad U_{p,1}\right) \tag{5b}$$

The j superscript is used to emphasize dependency of the DD observable vector $\mathbf{X}^j_f$ on the pivot SV here and whenever the pivot SV cannot be clearly devised from the context, and $U_{m,n}$ and I_n stand for the m-by-n integer matrix consisting of all ones and the n-by-n identity matrix, respectively. Because the same two pivot SV measurements appear in each of the p DD observables, their covariance matrix is full, that is,

$$\mathrm{cov}\left(\mathbf{X}^j_f\right) = \sigma^2_{Xf} D \;\; , \;\; D := T_{DD}T^T_{DD} = 2\left(U_{p,p} + I_p\right) \tag{6}$$

The core of this CDGPS approach to long-baseline relative positioning, which is frequently used in ground-based RTK techniques for baselines of tens of km, is thus the capability to produce fast, accurate, and robust solutions for carrier-phase integer ambiguities. To adapt it to space applications over baselines of hundreds of km, a purposely-designed dynamic-based filter carries out ambiguity resolution.

III. On the fly Ambiguity Resolution

Static initialization is not possible in satellite applications, so integer ambiguities must be resolved in kinematic conditions, i.e. on the fly. This is performed in the present work by integrating an EKF with an ILS estimator. The integration of the integer estimates into the float solution computed by the EKF presents many critical aspects, which can be dealt with in several ways [6]–[12]. The following subsections describe the strategy proposed by the present work to cope with this problem.

A. Float Estimates by EKF

The application of interest is described in the Earth Centered Earth Fixed (ECEF) reference frame by the following standard nonlinear stochastic model to suit the EKF estimation theory:

$$\begin{cases} \mathbf{x}_{k+1} = \boldsymbol{\eta}_k\left(\mathbf{x}_k\right) + \mathbf{w}_k \\ \mathbf{y}_k \quad = \mathbf{h}_k\left(\mathbf{x}_k\right) + \mathbf{v}_k \end{cases} \tag{7}$$

where $\mathbf{x}$ is the system state vector, $\mathbf{y}$ is the measurement vector, $\boldsymbol{\eta}$ is the non-linear state propagation function, $\mathbf{h}$ is the non-linear observation function, $\mathbf{w}$ is the process noise vector, $\mathbf{v}$ is measurement noise vector, and the subscript k is used to denote the variable's value at time t_k. Both $\mathbf{w}$ and $\mathbf{v}$ are assumed to be zero-mean white Gaussian noises, uncorrelated in time, mutually uncorrelated and uncorrelated with the state vector at the same time sample. The selected state and measurement vectors are

$$\mathbf{x} = \begin{pmatrix} \mathbf{b} \\ \vdots \\ \mathbf{VTEC} \\ \mathbf{a}^j \end{pmatrix}, \quad \mathbf{y} = \begin{pmatrix} \mathbf{P}_1^j \\ \mathbf{P}_2^j \\ \mathbf{L}_1^j \\ \mathbf{L}_2^j \end{pmatrix} \tag{8}$$

In Eq.(8), **VTEC** is the vector including the two vertical total electron contents above the receivers in TECU (Total Electron Content Unit, corresponding to 10^{16} electrons per square meter) and $\left(\mathbf{a}^j\right)^T = \left(\mathbf{a}_w^{jT} \quad \mathbf{a}_1^{jT}\right)$ stands for the estimated ambiguity vector including WL and L1 ambiguities. Because of the DD observables correlation in Eq.(6), the resulting measurements covariance matrix is block diagonal, i.e. $\mathrm{cov}(\mathbf{v}) = diag\left(\sigma_{P1}^2, \sigma_{P2}^2, \sigma_{L1}^2, \sigma_{L2}^2\right) \otimes D$, where $\otimes$ is the standard notation for Kronecker's product. The state vector is related to the measurements by means of the following observation model

$$h(\mathbf{x}) = U_{4,1} \otimes \mathbf{g}^j(\mathbf{b}) + \begin{pmatrix} A_V & A_a \end{pmatrix} \begin{pmatrix} \mathbf{VTEC} \\ \mathbf{a}^j \end{pmatrix} \tag{9}$$

which nonlinearly depends on the baseline via the double difference geometric terms $\mathbf{g}^j(b) = \begin{pmatrix} g^{j1} & \dots & g^{jp} \end{pmatrix}^T$. The observation model is instead linear w.r.t. the VTEC and the cycle ambiguities. The two matrices conveying the effects of the ionospheric delays and of the ambiguities are

$$A_V = \begin{pmatrix} 1 \\ -1 \end{pmatrix} \otimes \begin{pmatrix} 1 \\ \gamma^{-2} \end{pmatrix} \otimes T_{DD} \begin{pmatrix} 0 & \mathbf{m}_d \\ \mathbf{m}_c & 0 \end{pmatrix}, \; A_a = \begin{pmatrix} 0 & 0 \\ 0 & 0 \\ 0 & \lambda_1 \\ -\lambda_2 & \lambda_2 \end{pmatrix} \otimes I_p \tag{10}$$

The first term in the A_V equation is due to the opposite effect of dispersive delays on pseudorange and carrier phase measurements, the second term is due to the inverse square frequency dependency of first order ionospheric delays, and the remaining p-by-2 matrix maps the VTEC of the two receivers into the slant DD ionospheric delays on L1. The coefficients of this matrix are expressed as a function of non-differenced ionospheric delays, with $\mathbf{m}_{rec} = \begin{pmatrix} m_{rec}^1 & \dots & m_{rec}^p & m_{rec}^j \end{pmatrix}^T$ being the vector enclosing the Lear's isotropic mapping function [23],[24], which maps the vertical TEC of the receiver *rec* into the L1 ionospheric delays along the ray path coming from the SV *sv*, as follows.

$$m_{rec}^{sv} = \frac{40.3}{f_1^2} \cdot \frac{2.037}{\sin\left(E_{rec}^{sv}\right) + \sqrt{\sin^2\left(E_{rec}^{sv}\right) + 0.076}} \tag{11}$$

In Eq.(11), the L1 frequency shall be expressed in Hz, the unit of measurement of m_{rec}^{sv} is m^3/(number of electrons), and the mapping function depends on the elevation angle of *sv* with respect to *rec*, denoted by E_{rec}^{sv}, which depends on the *sv* and *rec* Earth-centered positions. As such, the ionospheric delay model introduces an additional nonlinearity in the observation model of Eq.(9), being the A_V matrix dependent on **b**.

In order to maintain accuracy and robustness in the floating estimate of DD ambiguities over long baselines, the ionospheric delay terms have been included in the filter state. However, differently from [7] and [25], the VTEC is assumed variable along the baseline [26]. When two different VTECs are considered for chief and deputy, the Lear's model is potentially able to approximate true DD ionospheric delays with a high correlation and a RMS error of a few

centimeters [23]. These features make it particularly suited for aiding the estimation of DD integer ambiguities in long-baseline relative navigation.

The observation model relating the state vector to the observables is thus nonlinear in **b** due to both the DD geometric range vector $\mathbf{g}^j$ and the mapping function. In addition, it does not depend on the baseline rate, and is linear in the remainder of **x**. Its Jacobian matrix, which is of interest in computing Kalman's gain, is thus given by

$$\frac{\partial \mathbf{h}}{\partial \mathbf{x}} = \begin{pmatrix} G & 0_{4p,3} & A_V & A_a \end{pmatrix} \tag{12}$$

The G term includes both the geometry and mapping function dependence on **b**. Nonetheless, for LEO altitudes and baselines in the order of few hundreds of kilometers, the dependence of the mapping function on the baseline vector is negligible with respect to the Jacobian $\partial \mathbf{g}^j / \partial \mathbf{b}$, thus

$$G \approx U_{4,1} \otimes \partial \mathbf{g}^j / \partial \mathbf{b} \tag{13}$$

The simple dependency of the DD geometric term on **b** allows an analytic closed-form expression for $\partial \mathbf{g}^j / \partial \mathbf{b}$. Denote as $\nabla_b \mathbf{g}^j_{\langle \kappa \rangle}$ the κ-th row of the $\partial \mathbf{g}^j / \partial \mathbf{b}$ matrix, which is equal by definition to the gradient w.r.t **b** of the κ-th DD geometric range. Carrying out the derivatives, the gradient can be shown to equal the difference of the LoS versors between the two SV forming the DD pair and the deputy receiver.

$$\nabla_b \mathbf{g}^j_{\langle \kappa \rangle} = \frac{\boldsymbol{\rho}_d^j}{\left\| \boldsymbol{\rho}_d^j \right\|} - \frac{\boldsymbol{\rho}_d^\kappa}{\left\| \boldsymbol{\rho}_d^\kappa \right\|} \tag{14}$$

The relative dynamics between the two satellites are modeled by a nonlinear Keplerian relative orbital motion augmented with J_2 effects and with additive process noise $\mathbf{w}_b$:

$$\ddot{r}_c = \qquad \qquad \dot{r}_c = \qquad \tag{15a}$$

$$C_1(\mathbf{r}_c) = 1 + \frac{3}{2} \frac{J_2 r_\oplus^2}{\langle \mathbf{r}_c, \mathbf{r}_c \rangle} - \frac{15}{2} \frac{J_2 r_\oplus^2}{\langle \mathbf{r}_c, \mathbf{r}_c \rangle^2} r_z^2 \tag{15b}$$

$$C_2(\mathbf{r}_c, \mathbf{b}) = -\frac{\|\mathbf{r}_c\|^3}{\sqrt{\left(\langle \mathbf{r}_c, \mathbf{r}_c \rangle + 2 \langle \mathbf{r}_c, \mathbf{b} \rangle + \langle \mathbf{b}, \mathbf{b} \rangle \right)^3}} C_1(\mathbf{r}_c + \mathbf{b}) \tag{15c}$$

where μ is the Earth gravitational constant, $r_\oplus$ is the Earth equatorial radius, J_2 is the second zonal harmonic, Ω_E is the Earth angular velocity vector in ECEF, r_z is the chief position vector's ECEF z-component, $\langle \cdot, \cdot \rangle$ indicates the scalar product, and $\times$ represents the vector product. The Jacobian of the considered dynamics model is not reported for the sake of brevity, but it can be computed analytically after trivial algebra.

The selected dynamics are a trade-off between complex but accurate trajectory propagation and a computational load adequate for real-time onboard implementation. The above model, being concerned with relative dynamics, allows modeling differential perturbations (e.g. differential drag) as process noise while keeping low the computational effort [27]. Indeed, formation flying satellites usually lie on orbits whose parameters slightly differ and have similar ballistic coefficients so to minimize control efforts to maintain the formation. This implies that differential perturbations are usually much smaller than absolute ones. Nonetheless, the application of the selected dynamic model requires the implementation of the absolute dynamics of the chief satellite. As absolute position errors do not contribute significantly to relative position ones, the same model is used to propagate also the absolute chief satellite position along with Eq.(15), resulting in a total of six second-order, nonlinear, ordinary differential equations (ODE). Solution of the ODE system is achieved using a 4th order Runge-Kutta integration method. In more detail, at each time instant t_k the GPS receiver of the chief satellite is supposed to compute its internal solution, i.e. chief satellite position and velocity. These are propagated forward in time along with $\mathbf{b}_k$ and $\dot{\ }$ to yield the predicted absolute and relative navigation solutions at t_{k+1}. However, only $\mathbf{b}_{k+1}$ and $\dot{\ }$ are retained in the filter's state vector. As time shifts to t_{k+1}, the chief satellite position is again computed as the internal receiver's solution. The chief absolute position needs not to be particularly accurate and the typical accuracy achieved by standard kinematic internal solutions based on pseudorange observables [21] allows the proposed approach to work. The relative dynamics model of Eq.(15) strictly holds for the baseline vector between the Center of Mass (CoM) of the two satellites, whereas GPS observables are relevant to GPS antennas phase centers. There are applications, such as the one presented in section V, for which the difference between these two baselines is sub-centimetric and can be ignored. In the more general case, compensating this effect might require knowledge of the spacecraft attitude.

At last, simple stochastic models are used for the remainder of the **x** vector. More precisely, the VTEC above the two receivers are modeled as two scalar first order Gauss-Markov processes with equal correlation time scale τ, whereas cycle ambiguities are modeled by a random constant plus random walk process.

$$\dot{\mathbf{VTEC}} = -\frac{1}{\tau}\mathbf{VTEC} + \mathbf{w}_v \quad , \quad (16)$$

Applying standard Kalman filter estimation theory to the models discussed throughout this section, the EKF generates a float estimate of the state vector, i.e. an estimate in which all the variables are estimated as real-valued, integer cycle ambiguities included. As for all recursive-filtering techniques, the state vector shall be initialized when the filter is first applied. Initial baseline and relative velocity are evaluated by differencing the position and velocity vectors of the chief and the deputy satellites, respectively, estimated as the standard single-epoch pseudorange solution of each receiver. DD integer ambiguities are initialized forming DD geometric ranges with these single epoch solutions and neglecting the ionospheric contribution. At last, the initial VTEC is set to zero for both the chief and the deputy satellite.

B. Fixed estimates by integrating ILS methods

The cycle ambiguities affecting DD carrier phase measurements are integer, but only a float estimate of their value is made available by the EKF. For taking advantage of the carrier phase measurements accuracy as in RTK methods, the integer nature of the ambiguities must be exploited. ILS estimators are able to search for an optimal vector of integers, starting from the float estimate of the ambiguity vector and the relevant covariance matrix. In particular, the Least-squares Ambiguity Decorrelation Adjustment (LAMBDA) method is the most used ILS estimator in GPS-based relative navigation applications, and is thus used in this paper. The IA estimates delivered by LAMBDA are discrete stochastic variables, whose probability mass function depends on the (Gaussian) probability density function (pdf) of the float estimates. In cases in which the float estimate pdf is sufficiently sharp to allow neglecting the stochastic nature of the LAMBDA integer estimates, these can be used to improve the *float* baseline vector estimate yielding the *fixed* solution. For simplicity and without loss of generality it is possible to consider a partition of the state vector **x** in which real-valued variables are separated from integer ones. Denote as **β** the vector comprising all the real-valued components of the state (i.e. the baseline, the baseline rate and the two VTECs in the present case). The fixed baseline and covariance matrix, conditioned on the fixed ambiguities, can be computed according to [28] as:

$$\breve{\boldsymbol{\beta}} = \hat{\boldsymbol{\beta}} - \hat{C}_{\beta a}\hat{C}_{aa}^{-1}\left(\hat{\mathbf{a}} - \breve{\mathbf{a}}\right) \; ; \; \breve{C}_{\beta\beta} = \hat{C}_{\beta\beta} - \hat{C}_{\beta a}\hat{C}_{aa}^{-1}\hat{C}_{a\beta} \quad (17)$$

where the symbols ˆ and ˘ refer to the float and fixed estimates, respectively, and C_{lz} stands for the covariance matrix between the generic variables l and z.

Whenever the float ambiguity estimates do not make it possible to neglect the stochastic nature of the integer estimates obtained by LAMBDA, Eq.(17) cannot be used for improving $\boldsymbol{\beta}$. Indeed, in presence of errors in the estimated IA, the fixed solution can be less accurate than the float one. Establishing the conditions in which the IA vector is suitable for being fixed or not is a non-trivial task [29]. In general, the fixed solution is computed only when the IA vector can be assumed correct with a certain confidence level. Several integer validation tests have been designed for this purpose and are customarily employed in relative positioning by CDGPS [30].

In real-time long-baseline applications, the dominating error sources are the DD broadcast ephemeris error and the residual DD ionospheric path delay. These errors exhibit a distinctive time-correlation and induce a non-zero bias in the ambiguity float estimate. The theoretical assumptions upon which the LAMBDA method and the integer validation tests are based do not hold in these applications. In order to employ the proposed low-fidelity computationally efficient float solution, time correlation of integer ambiguities shall be exploited as much as possible. More precisely, because the cycle ambiguities are constant in time for a specific DD pair, the fixed solution derived from Eq.(17) can also be fed back to the EKF for improving the float estimate at the following time instants, closing the loop between the float solution and the ILS estimator. This closed-loop arrangement, used in other precise relative positioning applications [7], [11], [12], [25], is able to further improve the fixed ambiguities estimate about the correct integer values despite the time-correlated ephemeris and ionospheric errors. However, while potentially capable of increasing the performance w.r.t. both a purely float and the standard fixing technique, the closed-loop scheme is less robust to erroneously fixed integer ambiguities. Wrong IA will affect the filter solution in all the following time instants, spoiling the quality of the estimation of future ambiguities. This might easily result into divergence of the solution, even for very low fail rates [7].

When using the closed-loop approach, the integer validation step becomes thus of crucial importance. Lacking the applicability of their basic assumptions, standard integer validation tests, handling the vector of ambiguities $\mathbf{a}$ as a whole, have already shown unsatisfactory performance in long baseline relative positioning of spaceborne receivers, even when fed with highly accurate float estimates [11]. For these reasons, they are not applicable in the present context. Partial integer ambiguity validation tests are concerned with discriminating between the single ambiguities, i.e. separating the correct from the incorrect ones within the $\mathbf{a}$ vector. Partial integer validation lacks a theoretical background [31], but thanks to the increase in IA fixing performance that can be gained, they are customarily employed in long-baseline applications, usually designing the validation tests by common sense and following

empirical guidelines (see [7], [11], [12], [17], [25]). These techniques have shown the potentials for substantially improving the integer fixing success rate in long baseline applications [17].

Based on the above observations, the technique proposed in this paper for performing on-the-fly ambiguity resolution is to augment the float estimate of the EKF by a closed-loop integer fixing scheme, in which the LAMBDA method yields integer ambiguity candidates which are screened by a custom-developed partial integer validation test. Integer validation is performed only on the wide-lane integer ambiguities $\mathbf{a}_w$, which are explicitly maintained in the EKF state vector in place of the usual L2 ones. More precisely, WL validation is performed by applying two different tests, which involve residuals of the float wide-lane ambiguity and of the Melbourne-Wubbena (MW) measurement combinations [32],[33]. Both tests introduce a maximum value, d_a and d_b, respectively, of the relevant residual for the integer estimate to be deemed correct. These two threshold values are two additional tunable parameters of the EKF whose value depends on the specific application case (see section V for the details). Float ambiguity residual is defined as the distance between the float and the integer ambiguity estimate, and is a widely used indicator in standard validation tests [30]. The other residual builds upon the MW observables. Let λ_n and λ_w be the narrow and wide-lane wavelengths [18], respectively. The MW observables are defined as:

$$\mathbf{MW} = \lambda_1^{-1}\left[\begin{pmatrix} -\lambda_n & -\gamma\lambda_n & \lambda_w & -\gamma\lambda_w \end{pmatrix} \otimes I_p\right] \cdot \mathbf{y} \tag{18}$$

Combining the above definition with the observation model in Eq.(9), the MW combinations can be proved to allow direct sampling of the WL ambiguities, i.e. $\mathbf{MW} = \lambda_w \mathbf{a}_w$. Partial validation of the WL ambiguities is performed by screening the individual ambiguities with the validation tests. Let $a_{w\langle\kappa\rangle}$ be the κ-th component of the WL ambiguity vector and $n_{w\langle\kappa\rangle}$ its integer counterpart. The κ-th fixed WL is equal to the relevant integer estimate provided by LAMBDA only in case both validation tests are passed, that is

$$\breve{a}_{w\langle\kappa\rangle} \begin{cases} n_{w\langle\kappa\rangle} & \text{if } \left|n_{w\langle\kappa\rangle} - \hat{a}_{w\langle\kappa\rangle}\right| \le d_a \wedge \left|n_{w\langle\kappa\rangle} - MW_{\langle\kappa\rangle}/\lambda_w\right| \le d_b \\ \hat{a}_{w\langle\kappa\rangle} & \text{otherwise} \end{cases} \tag{19}$$

It is worth noting that the first test is influenced by the EKF float ambiguity estimates while the second only depends on the measurements. Because erroneous fixed IA could potentially corrupt the EKF float estimate in closed-loop schemes, the MW residual test is instrumental in limiting possible divergence of the solution and is essential for proper operation of the closed-loop filter.

Even though this paper makes no attempts to advance the theory in partial integer validation of ILS solutions, the proposed validation test has an intuitive theoretical justification. More specifically, partial validation of the components of the **a** vector would be possible with no theoretical difficulties in case the screened individual ambiguities would be uncorrelated. Previous results [34],[35], suggest that the wide-lane ambiguities estimates have almost uncorrelated variance, especially when residuals in DD ionospheric delay compensation are non-negligible w.r.t. a threshold value depending upon the code measurement noise. In long-baseline applications, the magnitude of DD ionospheric delays residuals when using Lear's model is in the order of several centimeters [23], well above the threshold values presented in [35]. Thus, WL ambiguities can be reasonably screened individually by partial integer validation tests in such applications. This strategy allows exploiting the advantages of the closed-loop scheme, by incorporating as much correct WL ambiguities as possible into the fixed solution thanks to their correlation properties, while minimizing the fail rate thanks to the precision of WL ambiguity float estimates. These considerations do not hold for L1 ambiguities that cannot be screened individually with satisfactory confidence and therefore are kept as floats in the EKF.

Validated WL ambiguities are modeled as deterministic variables, and can be then used to calculate the fixed solution by Eq.(17). As shown in Fig. 2, the fixed solution is used to replace the EKF state vector and covariance matrix for the prediction step of the next time epoch. After the fixing step, fixed WL integer ambiguities become part of the ambiguity resolution's output vector $\tilde{} = (\tilde{} \quad \tilde{}$. Being modeled as deterministic variables, fixed WL integer ambiguities have no correlation with any component of the fixed state vector $\breve{}$ and do not need to be further retained in the EKF.

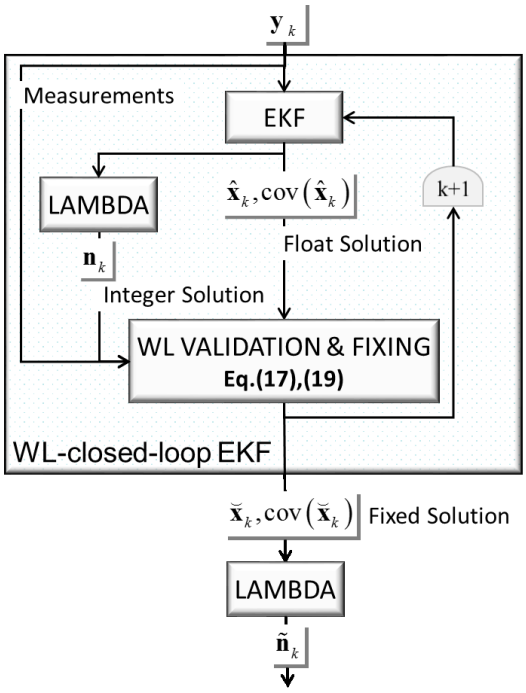

Fig. 2 Ambiguity resolution logic

Because of the WL validation, fixed solution includes validated WL integer ambiguities and not validated WL and L1 ambiguities, which are real numbers. For de-biasing the ionospheric-free carrier-phase observations both WL and L1 integer estimates are required. A secondary estimation by LAMBDA is thus performed (see Fig. 2), processing only L1 ambiguities with a validated WL counterpart. The resulting L1 integers are then kept into the ambiguity resolution output $\tilde{\ }$. Note that these L1 integers are computed on a single-epoch basis. If this secondary LAMBDA fails to estimate correctly some L1 ambiguities at a certain time epoch, this does not imply that the error will propagate forward in time, as opposed to what happens to WL ambiguities validated within the closed-loop scheme. The fail rate of L1 ambiguities, which is defined as the probability that the integer ambiguities are not correct, is thus controlled by the accuracy of the fixed solution. Being conditioned on the validated WL ambiguities, the fixed solution accuracy is assumed to be sufficient for limiting the fail rate to few percentage points, which is a generally accepted value [30].

IV. Kinematic relative positioning

As previously discussed, a highly accurate kinematic solution can be computed using the vector of integer ambiguity estimates $\tilde{\ }$ determined by the on-the-fly ambiguity resolution technique. For exploiting the carrier phase measurement accuracy as in RTK techniques, these integer estimates shall be used to compensate for the cycle ambiguity biases in the ionospheric-free carrier phase measurements as in Eq.(4).

The p double-difference, ionospheric-free carrier-phase observables, denoted by $\mathbf{L}_{IF}$, can be expressed as a linear function of the measurement vector $\mathbf{y}$. Recall that $\mathbf{L}_{IF}$ do not allow direct sampling of the DD geometric terms, unless they are de-biased of the cycle ambiguity term using the $\tilde{\imath}$ vector. Because of the partial integer validation tests, the $\tilde{\imath}$ vector will, in general, comprise q WL integer ambiguities and the corresponding q L1 ones, with $q \leq p$. Letting $\mathbf{L}'_{IF}$ be the part of the $\mathbf{L}_{IF}$ vector that can be de-biased, the following holds.

$$\mathbf{L}'_{IF} = T_{IA}\left\{\left[\frac{1}{1-\gamma^2}\begin{pmatrix}0 & 0 & 1 & -\gamma^2\end{pmatrix}\right]\otimes I_p\right\}\cdot\mathbf{y} \tag{20a}$$

$$\operatorname{cov}\left(\mathbf{L}'_{IF}\right) = \sigma_L^2\frac{1+\gamma^4}{\left(1-\gamma^2\right)^2}D' \tag{20b}$$

In Eq.(20a) the term in square brackets forms ionospheric-free carrier phase measurements combinations from the standard four $\mathbf{P}_1, \ldots, \mathbf{L}_2$ observables. In order to be applied to the measurements vector $\mathbf{y}$, which includes observations of all the p DD SV couples, it is necessary to inflate it to the appropriate dimensions by the Kronecker product. At last, $T_{IA} : \mathbb{R}^p \rightarrow \mathbb{R}^q$ stands for the linear transformation (and associated matrix) that allows extracting the q DD pairs for which integer estimates of L1 and WL ambiguities exist from all the p ones.

The covariance of $\mathbf{L}'_{IF}$ can be readily obtained from the one of the $\mathbf{y}$ vector applying linear algebra and Kronecker product properties, where D' is the q-by-q matrix having the same structure of D in Eq.(6). Substituting for $\gamma = 60/77$ one gets the well-known results that ionospheric-free combinations have a standard deviation that is about three times the one of uncombined DD measurements, which is in the order of the centimeter for modern GPS receivers (see [11] and the references therein). Defining

$$\mathbf{y}' = \mathbf{L}'_{IF} - \Delta\mathbf{L}'_{IF}\ ;\ \Delta\mathbf{L}'_{IF} = \frac{\lambda_1}{1-\gamma^2}\left[\begin{pmatrix}\gamma & 1-\gamma\end{pmatrix}\otimes I_q\right]\cdot\tilde{\imath} \tag{21}$$

one obtains a vector $\mathbf{y}'$ of de-biased measurements that, being the integer ambiguities modeled as deterministic variables, have the same covariance of $\mathbf{L}'_{IF}$. Unlike $\mathbf{L}'_{IF}$, $\mathbf{y}'$ allows sampling directly the DD geometric term of the relevant q DD pairs. Indeed, combining the definition of $\mathbf{y}'$ with the observation model in Eq.(9) results in $\mathbf{y}' = \mathbf{g}'(\mathbf{b})$ where $\mathbf{g}' = T_{IA}\cdot\mathbf{g}$.

A baseline estimate can be computed based on this model using a single-epoch kinematic filter, applying a Weighted Least Square (WLS) algorithm that processes $\mathbf{y}'$ at each time epoch. For applying the WLS algorithm, the nonlinear model is linearized about the best available estimate of $\mathbf{g}'$, obtained using the fixed baseline estimate $\breve{\mathbf{b}}$, and using the analytical Jacobian in Eq.(14). Letting

$$\Delta\mathbf{y}' = \mathbf{y}' - \mathbf{h}\left(\breve{\mathbf{b}}\right), \quad G' = \left.\frac{\partial \mathbf{h}}{\partial \mathbf{b}}\right|_{\breve{\mathbf{b}}} \qquad \Delta\mathbf{b} = \mathbf{b} - \breve{\mathbf{b}}; \tag{22a}$$

yields

$$\Delta\mathbf{y}' = G'\Delta\mathbf{b} \tag{22b}$$

Provided that the above linear system is over-determined, i.e. $q \geq 4$, an epoch-wise estimate of the correction $\Delta\tilde{\mathbf{b}}$ (necessary for improving $\breve{\mathbf{b}}$ to obtain the kinematic baseline $\tilde{\mathbf{b}}$) can be obtained as the WLS solution of the above linear system, using the inverse of $\mathbf{y}'$ covariance matrix as the weighing matrix.

$$\Delta\tilde{\mathbf{b}} = \left[G'^{T}\left(\mathbf{L}'_{IF}\right)^{-1}G'\right]^{-1}G'^{T}\left(\mathbf{L}'_{IF}\right)^{-1}\Delta\mathbf{y}' \tag{23a}$$

$$\mathrm{cov}\left(\Delta\tilde{\mathbf{b}}\right) = \left\{G'^{T}\left[\mathrm{cov}\left(\mathbf{L}'_{IF}\right)\right]^{-1}G'\right\}^{-1} \tag{23b}$$

The accuracy of the kinematic baseline depends on several factors. Even assuming the integer ambiguities and the observation model in Eq. (22) to be correct, the ranging measurements $\mathbf{y}'$ would be corrupted by a white noise term with a covariance given by Eq.(20). Additional effects, however, shall be taken into account. First, the integer estimation can have a limited, although hopefully negligible, fail rate. The most likely error of this kind is in missing the L1 ambiguity term of one wavelength, which thus causes a ranging error of about 20 cm. Furthermore, the observation model in Eq.(22) does not account for all systematic errors, i.e. time-correlated non-Gaussian stochastic processes, most notably the DD broadcast ephemeris error. Previous results on spaceborne GPS receivers' flight data suggest that broadcast ephemeris errors are the limiting factor in obtaining accurate absolute positions [21]. Results on relative positioning over long baselines using actual flight data, presented in the next section, suggest that broadcast ephemeris can induce errors in the order of centimeters in the DD range $\mathbf{y}'$, and are thus a limiting factor in these applications as well. The overall accuracy of the kinematic solution depends on how these ranging errors are mapped onto the three dimensional baseline. The amplification of ranging errors is governed by the G' matrix Dilution of

Precision (DOP), which, in turn, depends on the relative geometry of the q observations via Eq.(14). For typical DOP values, the kinematic baseline can be expected to be accurate at least at the cm-level considering only the measurement noise, but is typically much better [36]. As the DOP generally improves as the number q of G′ rows increases, the kinematic baseline is not computed when $q < 4$, to avoid further discriminating between the geometry of the observations for simplicity. In this case, the EKF fixed baseline $\breve{\boldsymbol{\rho}}$ becomes the best available estimate, and is used for avoiding data gaps in the relative position solution.

V. Application Case: Relative Positioning of GRACE satellites

A. Approach for performance assessment

Relative positioning performance of the developed CDGPS scheme is evaluated using GPS flight data acquired by the GRACE mission [37]. The mission consists of two identical satellites in near circular orbit at approximately 500 km altitude and 89.5 degrees inclination, separated from each other by about 220 km along-track in nominal conditions. The satellites are linked by a highly accurate K-Band microwave Ranging (KBR) system. In addition, each satellite also carries identical NASA JPL BlackJack dual frequency geodetic grade GPS receivers [38], attitude sensors and high precision accelerometers. A post-processed version of GRACE data and measurements, named Level 1B (L1B) data [39], is made available to the scientific community by JPL Physical Oceanography Distributed Active Archive Center (PODAAC). GPS L1B data employed in the present work consist of a full set of dual frequency carrier-phase and pseudorange measurements at a 0.1 Hz data rate, including code observations on L1 frequency and semi-codeless tracking on L2 frequency. Data editing is performed to set the elevation mask to 10 degrees and to detect and remove outliers in the GPS measurements. Broadcast ephemeris distributed by the International GNSS Service (IGS) are considered to reproduce real-time onboard operations.

L1B GRACE data products are also used, along with IGS final products, to generate reference data, which are exploited to quantify the performance of the CDGPS scheme. These reference data include the magnitude of the baseline vector, the baseline components, the DD ionospheric delays, ephemeris error, and the DD integer ambiguities. In particular, KBR data have been used to calculate the reference baseline magnitude. The KBR instrument measures the change in distance between the satellites with a precision of 10 μm and 0.2 Hz rate. The reference baseline magnitude can be estimated accordingly by a specially designed procedure [36]. L1B products include also a GPS Navigation (GNV) data product, which contains an estimate of the two spacecraft CoM position and velocity vectors every 1 minute. These estimates are obtained as the result of a precise orbit determination tool [39], and typically have

a time-varying accuracy of a few centimeters in position, which is not negligible with respect to the order of magnitude of the expected estimation error of the kinematic filter. The baseline vector estimation error, obtained by difference with GNV data at their reduced rate of 1/60 Hz, is thus less truthful than its magnitude error. Reference values for integer ambiguities, DD ionospheric delays, and GPS SV positions are also computed for gaining further insight into the performance of the positioning technique. Taking advantage of the accurate knowledge of DD geometric ranges given by KBR data, GNV data, and final IGS products, high-accuracy estimates of integer ambiguities and ionospheric delays can be obtained. The implemented procedure is not discussed here for brevity and is described in [23], to which the interested reader can refer. Ephemeris error is also estimated by comparing broadcast GPS SV positions with final IGS products.

According to KBR and GNV data, the baseline between the spacecraft CoM can be estimated, whereas the CDGPS scheme calculates the baseline between the phase centers of the GPS antennas. Therefore, the GPS antenna offset with respect to CoM is compensated taking into account the attitude of both satellites, which is provided within L1B products as Star Camera Assembly (SCA) data. GPS antennas on board GRACE satellites have a phase center offsets of about 41 cm along the z-axis of the body reference frame, which is actively controlled and is mainly directed towards the local nadir. Hence, the baseline components between the phase centers of the GPS antennas deviate less than a few mm from those between CoMs. Centimetric relative positioning would thus have been possible even neglecting GPS antenna offsets. Clock solutions are also provided within L1B data. More precisely, L1B data are time tagged to GPS time using post-processed clock solutions computed at a 0.1 Hz data rate. GRACE GPS measurements are therefore not affected by the residual timing errors that would be experienced in real-time onboard CDGPS. Anyway, as discussed in section II for the reference receivers, the effect of residual timing errors is definitely smaller than broadcast and differential ionospheric errors, which makes the selected GRACE dataset suitable to assess the performance of the developed filtering approach.

B. One-day long dataset

The developed approach has been tested on a one-day long time span. More specifically, the Day Of Year (DOY)18, 2009 has been considered in which the satellites reached their maximum distance of about 270 km. While this choice allows maximizing DD error terms, in general, January 2009 corresponds to a minimum in the solar cycle, and, thus, in the ionosphere electron content. Performance over different ionospheric conditions is evaluated in the next section. Filtering of the complete one-day-long dataset took less than 5 minutes to be completed in Matlab® by a

standard desktop PC equipped with a Pentium® IV 2.4 GHz processor and 2GB RAM. The execution time is less than 0.4% the simulated time span, suggesting that the computational load is more than adequate to cope with onboard real-time computational requirements.

The calculation of the integer ambiguities by the dynamic filter requires setting specific tunable parameters. The majority of these parameters deals with EKF implementation and thus comprises measurement noise standard deviations (STD), state vector initial STD, and process noise STD associated to the selected dynamic models. In addition to EKF-related parameters, the thresholds for carrying out the validation of WL ambiguities must be assigned. Table 1 lists the selected values for the tunable parameters, where cycles units are referred to the corresponding ambiguity, i.e. if the parameter refers to WL (L1) ambiguity the unit is the WL (L1) cycle. The tuning of the EKF has been performed by a conventional trial and error procedure, aimed at maximizing the number of fixed ambiguities while minimizing the percentage of wrong integers. A single standard deviation is used for dual frequency carrier-phase observations. Indeed, even if the noise measurement should be lower on carrier phase observations of the L1 code than on the semi-codeless tracking of the L2 frequency [20], this difference has no practical effect on the performance of the filter up to centimetric accuracy.

Table 1. Value of tunable parameters used within the filter

	Parameter	Value
Measurement noise STD	Pseudorange (L1)	0.2 m
	Pseudorange (L2)	0.25 m
	Carrier-phase	0.005 m
Initial STD	Baseline	0.7 m
	Baseline Rate	0.03 m/s
	VTEC	4 TECU
	IA WL	10^4 cycles
	IA L1	10^4 cycles
Process noise STD	Base. Acc.	$7 \cdot 10^{-5}$ m/s^2
	VTEC STD	1.3 TECU/s
	VTEC τ	3 s
	IA WL	10^{-4} cycles/s
	IA L1	10^{-3} cycles/s
WL IA validation	Float test	0.35 cycles
	MW test	0.28 cycles

Fig. 3 reports the correlation between the reference DD ionospheric delays and those estimated by the filter. Positive correlation is apparent and DD ionospheric delays are estimated with a root mean square (RMS) error of about 4 cm, despite maximum values of about 0.5 meters. The EKF is able to evaluate all the DD ionospheric delays

with an accuracy of about 6 cm in 90% of the cases (see Fig. 4). The capability of reducing the biasing contribution coming from differential ionospheric delays up to a value that is only a fraction of the L1 wavelength is a key factor for supporting the resolution of integer ambiguities.

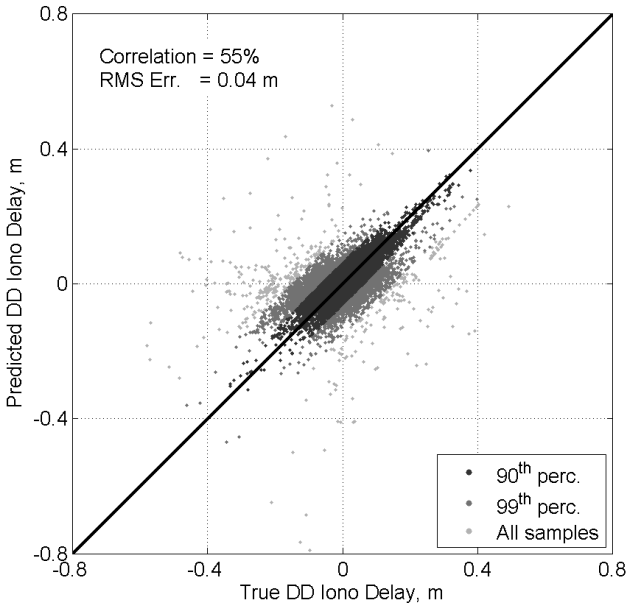

Fig. 3 Correlation between reference and predicted DD ionospheric delays.

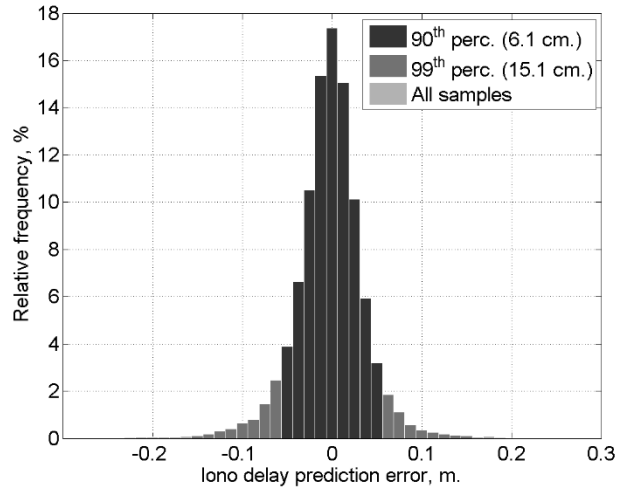

Fig. 4 DD ionospheric delays prediction error distribution.

Ambiguity estimation performance suggests that the ionosphere model is indeed effective. More precisely, the wide-lane ambiguities are fixed in more than 98% of the cases. The WL ambiguities fail rate is null over a one-day long time span, whereas a 3.6 % fail rate is achieved for L1 ambiguities. Compared with typical performances of both real-time and post-processing terrestrial and satellite ambiguity resolution schemes (e.g. [11], [17], and [30]), the ambiguity estimation performance can be considered quite sharp: the fixing rate is 98%, of which less than 2% are

wrong. In addition, such fail rate has no impact on the filter stability since L1 ambiguities are validated outside the dynamic filter. The time profile of the percentage of fixed ambiguities out of the total is shown in Fig. 5. Results show that the greatest part of the ambiguities are fixed instantaneously as they appear in the observation equations, at most within a 2 or 3 time epochs, i.e. within 30 seconds. The majority of unfixed ambiguities concentrates in three periods of the day, each about twenty-minutes long, in which the observation conditions let the WL validation test in Eq.(19) be more selective.

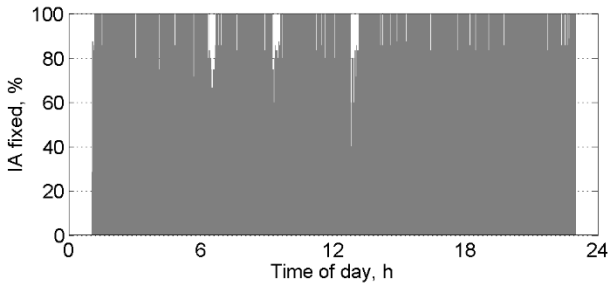

Fig. 5. Percentage of fixed cycle ambiguities.

Fig. 6 shows the baseline magnitude error obtained comparing the solutions of the developed CDGPS scheme with the highly accurate KBR one. The kinematic solution is shown for $q \geq 4$, that is, whenever the number of fixed ambiguities allows for de-biasing at least four ionospheric-free carrier-phase observables. The kinematic algorithm can be applied in more than 96 % of time epochs thanks to the high capability to correctly fix integer ambiguities. In the remaining time epochs, the fixed baseline solution generated by the dynamic filter, shown in Fig. 6 as well, is available as a backup to avoid data gaps. The closed-loop EKF solution is in general worse than the kinematic one, being affected by both orbital dynamics and ionospheric delay error terms, which are instead compensated for by fixing L1 ambiguities in the kinematic approach. The kinematic baseline approximates the reference baseline magnitude with a RMS error of about 4 cm and a maximum error below 40 cm in spite of a baseline of almost 270 km.

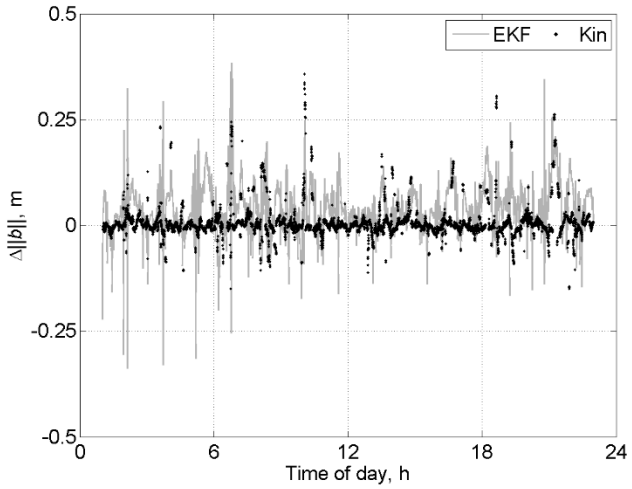

Fig. 6 Baseline magnitude estimation error.

As previously discussed, the residual error present in the kinematic solution is due to un-modeled systematic ranging errors, most notably erroneous compensation of the cycle ambiguity term and DD broadcast ephemeris error, which are amplified by the observation geometry via the G' matrix of Eq.(22). Fig. 7 compares the residual error of the kinematic solution to the ephemeris error. Data are shown only in the radial direction, whose error is generally worse than along- and cross-track errors. Because of the very low ambiguity fail rate, the residual error is mostly due to the broadcast ephemeris, amplified by the radial DOP coming from the G' matrix. The three components of the vector estimation error are reported in Fig. 8, along with their three-sigma bounds computed by the filter. Results suggest that the vector relative positioning performance is higher in the cross-track direction and worse in the radial one, due to GPS observation geometry. Being the latter modeled within the kinematic solution, the filter is capable of predicting the expected error, which is within three sigma bound in most cases. All three components are estimated with a RMS error in the order of some centimeters. Table 2 summarizes the performance achieved by the proposed algorithm over the selected one-day long dataset.

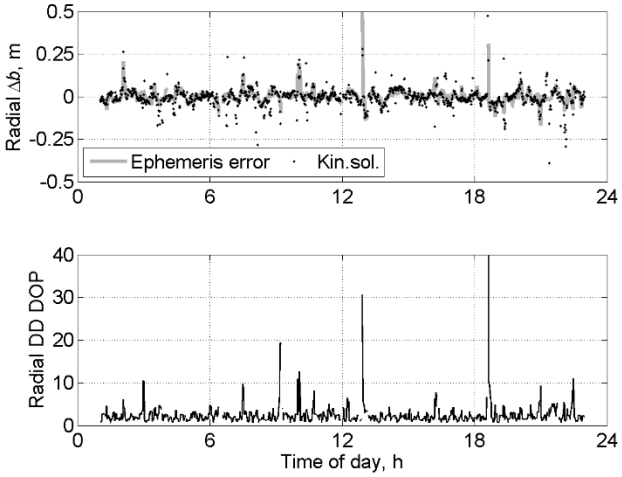

Fig. 7 Radial baseline estimation error and dilution of precision.

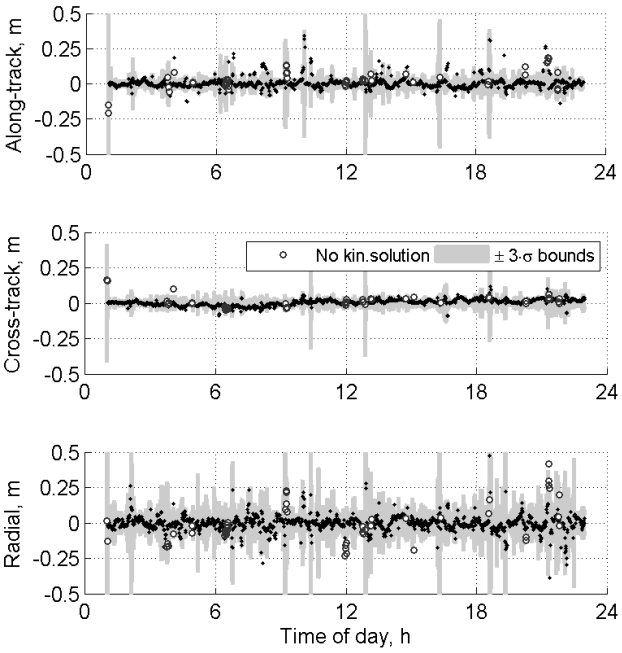

Fig. 8 Baseline estimation error components.

Table 2. Relative positioning performance over one-day long dataset

Baseline Component	Estimation Error	
	Max, cm.	*RMS, cm.*
Magnitude (||*b*||)	35.8	4.2
Along Track	34.0	4.3
Cross Track	16.1	2.4
Radial	83.4	6.8
Kin. Solution Availability	96.3 %	
Ambiguity	**IA Estimation**	
	Fixing Rate, %	*Fail Rate, %*
WL	98.0	0.0
L1	98.0	3.6
All	98.0	1.8

C. Robustness to different operating conditions

This section addresses the robustness of the proposed CDGPS scheme to different operating conditions. More precisely, the filter performances are here evaluated under various observation geometries and for different solar activity levels.

The observation geometry depends on the position of the GRACE satellites w.r.t. the GPS constellation. While the GPS constellation is phased w.r.t. Earth's rotation, the GRACE satellites are not, making the observation conditions aperiodic. A one-week long dataset, ranging from DOY12 to DOY19, 2009, is used to reproduce a reasonable amount of different observation conditions. For making the results comparable across DOYs, the filter is run on each one-day long dataset separately. Fig. 9 reports the fixing and fail rates of integer ambiguities together with the percentage of time epochs in which the kinematic solution is available. The fixing rate is always higher than 96% with fail rates always under 5%, thus making it possible to calculate the kinematic solution in more than 95% of the time epochs. The overwhelming majority of DD ambiguities are resolved in less than a few time epochs and the time to first kinematic fix is less than 20 seconds in all the dataset, except in DOY19 in which it takes 2 minutes to fix 4 pairs of WL and L1 ambiguities, due to an unfavorable observation geometry. As shown in Fig. 10, the baseline magnitude is estimated with RMS and maximum errors in the order of 10 cm and 1 meter at most, respectively. The capability to get a stable and robust relative positioning solution under different observation geometries is thus clearly demonstrated.

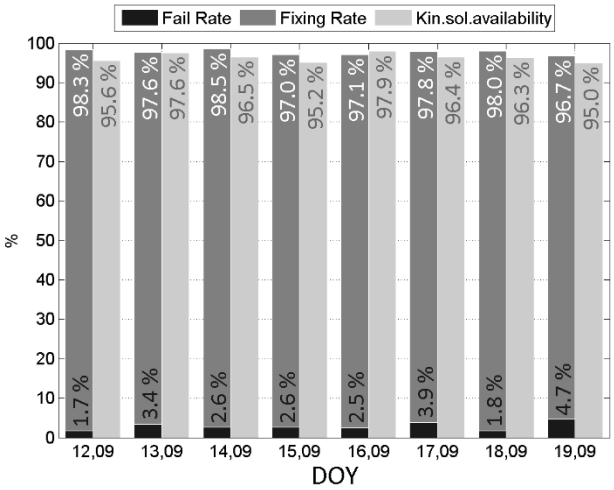

Fig. 9 Kinematic solution availability time epochs, ambiguities fixing and fail rates.

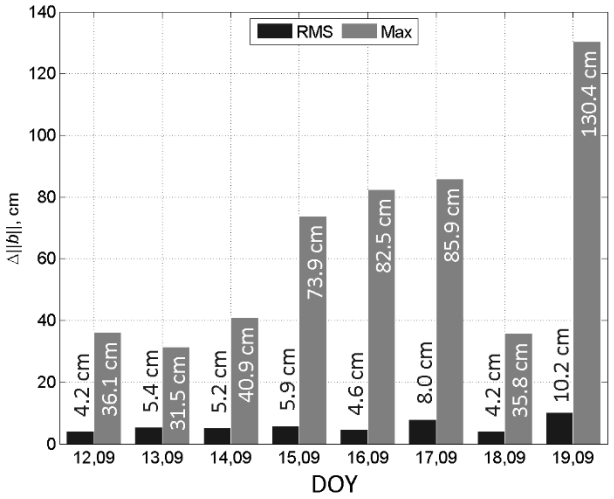

Fig. 10 Baseline magnitude RMS and maximum estimation error.

All previous results refer to DOYs near the minimum of the solar cycle, in which the magnitude of ionospheric delays is generally minimum. The filter's sensitivity to ionospheric conditions is assessed by evaluating the relative positioning performances across different phases of the solar activity. Table 3 shows the features of four one-day-long datasets chosen to represent the spectrum of possible ionospheric conditions. DD delays magnitude depends on the baseline and on the VTEC values characterizing the ionosphere above the receivers' altitude. The maximum VTEC estimated by the filter in January 2009 is in the order of 10 TECU, which, according to IGS final products, corresponds to maximum VTEC values on ground of about 30 TECU. With respect to January 2009, the other DOYs in Table 3 provide ionospheric conditions ranging from typical (for DOY298, 10 and DOY88, 11) to intense for DOY304, 2011, which occurs near a local maximum in the ionospheric mean TEC. VTEC values of almost 110 TECU were recorded

on ground for DOY304, which result in a maximum DD ionospheric delays at GRACE altitude of about 6.5 meters, well above the 0.5 m of January 2009.

Table 3. Datasets for evaluating sensitivity to ionospheric conditions.

DOY	Max. ‖b‖, km	Max. Ground VTEC, TECU	Max. $VTEC_c$, TECU	Max. L1 DD iono-delay, m.
18, 2009	268	31	8.7	47.9
298, 2010	236	58	15.6	173.6
88, 2011	217	75	26.4	222.9
304, 2011	241	107	51.0	659.8

The filter's performance in these four DOYs is shown in Fig. 11. In DOY304,11 the filter has been retuned w.r.t. January 2009 case for dealing with delays one order of magnitude higher, mainly increasing the VTEC process noise. Indeed, because of Lear's model inaccuracies, the higher magnitude of the ionospheric delays causes a correspondingly higher ionospheric residual error in the EKF. The overall effect is to increase the ambiguity fail rate up to about 15%. However, as in January 2009, the majority of WL ambiguities is still estimated correctly, and the higher fail rate concerns the L1 ambiguities. This allows computing the kinematic solution in most time epochs, even in intense ionospheric conditions. The fail rate's increase causes a proportional increase in the baseline RMS and maximum estimation error. To a first order, the degradation of all these three performance metrics is proportional to the increase in the VTEC values above the receivers' altitude (see Fig. 12), except for DOY304,11. In these intense ionospheric conditions, the quality of the L1 integer ambiguity solution, and thus of the baseline estimation, is substantially degraded by the errors in compensating DD delays of several meters. Hence, the working assumption that the fixed solution accuracy is sufficient for ignoring the ambiguity fail rate might not be fully applicable in these intense ionospheric conditions. Nonetheless, the filter's structure, based on single-epoch, open-loop fixing of L1 ambiguities, prevents divergence of the solution. This enhanced stability in relative positioning is a highly desirable property for real-time onboard operations.

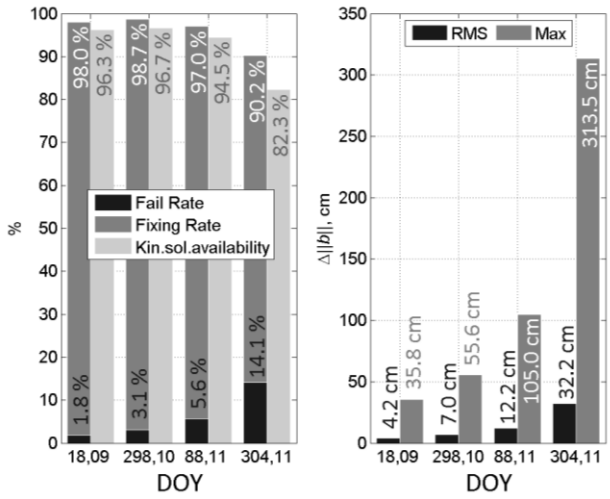

Fig. 11 Filter's performances under various ionospheric conditions.

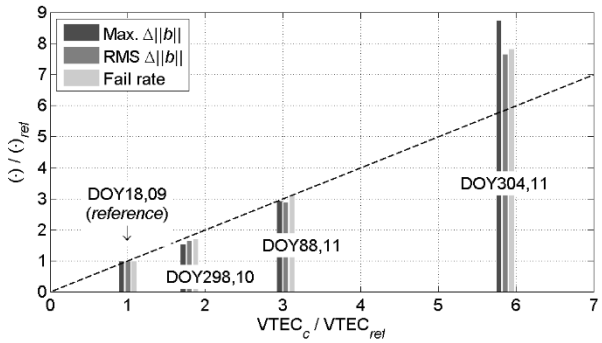

Fig. 12 Filter's performance trend vs, chief's VTEC. DOY18,09 is taken as a reference.

VI. Conclusion

An original approach for relative positioning of a formation of two satellites in low Earth orbit using the Global Positioning System has been presented. The approach is specifically designed for decimeter-level real-time onboard relative positioning in applications where a large inter-satellite separation, in the order of some hundreds of kilometers, is required. To preserve a high relative positioning accuracy in spite of the long baseline, the proposed approach performs the integer ambiguities resolution separately from the computation of the relative position. The ambiguities solution is provided by an Extended Kalman Filter coupled with an Integer-Least-Squares estimator. The relative position is instead obtained with high precision as the solution of a conventional kinematic least-square algorithm, processing ionospheric-free combinations of carrier-phase measurements de-biased of the integer ambiguities computed in the previous step. The approach accuracy and robustness have been verified on real-world measurements coming from the Gravity Recovery and Climate Experiment mission, consisting of two identical satellites in near

circular orbit with a nominal separation of 220 km. For testing the approach, a full dataset of dual frequency carrier-phase and pseudorange measurements at 0.1 Hz data rate has been used.

Approach performance in the relative positioning has been verified first with reference to a one-day long dataset relevant to a condition of maximum separation between the two satellites, i.e. about 270 km. Results clearly demonstrate the capability of the dynamic filter to estimate double-difference ionospheric delays with accuracy adequate to support a correct evaluation of DD integer ambiguities. This result is also confirmed by the capability of the filter of performing fast and reliable on the fly ambiguity resolution: the ambiguities fixing rate is about 98%, with a fail rate smaller than 2%. In addition, the most part of the ambiguities is fixed instantaneously. Thanks to the high capability to fix correctly the integer ambiguities, the kinematic filter can be applied in more than 96% of the time epochs, yielding a baseline magnitude estimate with a root-mean-square error of 4 cm and a maximum error below 40 cm.

Robustness to observation conditions and ionospheric activity has also been assessed by using different datasets. The capability to get a stable and reliable relative position solution as the observation conditions vary is clearly demonstrated. Results also suggest that the relative positioning and ambiguity estimation accuracy are proportional to the electron content above the receivers. During intense ionospheric activity, the filter operates in limit conditions for the applicability of its underlying assumptions. Nonetheless, thanks to its mixed dynamic – kinematic structure, filter estimates degrade gracefully despite an increase of double-difference ionospheric delays of more than one order of magnitude.

VII. References

[1] Krieger, G., and Moreira, A., "Spaceborne bi- and multistatic SAR: Potential and challenges," *Institute of Electrical Engineers Proceedings – Radar, Sonar and Navigation*, Vol.153, No.3, June 2006, pp.184,198.

[2] D'Errico, M., and Fasano, G., "Design of interferometric and bistatic mission phases of COSMO-SkyMed constellation," *Acta Astronautica*, Vol.62, No.2-3, January–February 2008, pp.97-111.

[3] Renga, A. Moccia, A., D'Errico, M., Dellepiane, S., Angiati, E., Vernazza, G., et al., "From the expected Scientific Applications to the Functional Specifications, Products and Performance of the SABRINA missions", *Proceedings of the IEEE Radar Conference*, Rome, Italy, 2008, pp. 1117-1122.

[4] Gill, E., and Runge, H., "Tight formation Flying for an along-track SAR interferometer," *Acta Astronautica*, Vol.55, No.3-9, August–November 2004, pp.473 – 485.

[5] Peterson, E.H., Zee, R.E., and Fotopoulos, G., "InSAR Microsatellite Constellations Enabled by Formation Flying and Onboard Processing Capabilities," *Proceedings of the 25th AIAA/USU Conference on Small Satellites,* 2011.

[6] Montenbruck, O., D'Amico, S., Ardaens, J. S., and Wermuth, M., "Carrier phase differential GPS for LEO Formation Flying - The PRISMA and TanDEM-X Flight Experience," *American Astronautical Society Astrodynamics Specialist Conference*, Girdwood, USA, August 2011.

[7] Leung, S., and Montenbruck, O., "Real-Time Navigation of Formation-Flying Spacecraft Using Global-Positioning-System Measurements," *Journal of Guidance, Control, and Dynamics*, Vol. 28, No. 2, March–April 2005, pp. 226-235.

[8] Ebinuma, T., Bishop, R.H., and Glenn Lightsey, E., "Integrated hardware investigations of precision spacecraft rendezvous using the global positioning system," *Journal of Guidance, Control, and Dynamics*, Vol.26, No. 3, May-June 2003, pp. 425-433.

[9] Mohiuddin, S., and Psiaki, M. L., "Carrier-Phase Differential Global Positioning System Navigation Filter for High-Altitude Spacecraft," *Journal of Guidance, Control, and Dynamics*, Vol. 31, No. 4, July-August pp. 801-814, 2008.

[10] Wolfe, J. D., Speyer, J. L., Hwang, S., Jae Lee, Y., and Lee, E., "Estimation of Relative Satellite Position Using Transformed Differential Carrier-Phase GPS Measurements," *Journal of Guidance, Control, and Dynamics*, Vol.30, No.5, September-October 2007, pp. 1217-1227.

[11] Kroes, R., Montenbruck, O., Bertiger, W., and Visser, P., "Precise GRACE baseline determination using GPS," *GPS Solutions,* Vol.9, No.1, April 2005, pp 21-31.

[12] Wu, S-C., and Bar-Sever, Y.E., "Real-Time Sub-cm Differential Orbit Determination of Two Low-Earth Orbiters With GPS Bias Fixing," *Proceedings of the 19th International Technical Meeting of the Satellite Division of The Institute of Navigation* (ION GNSS 2006), Fort Worth, TX, September 2006, pp. 2515-2522.

[13] Ardaens, J.S., and D'Amico, S., "Spaceborne Autonomous Relative Control System for Dual Satellite Formations," *Journal of Guidance, Control, and Dynamics,* Vol.32, No.6, November–December 2009, pp. 1859-1870.

[14] Montenbruck, O., Ebinuma, T., Glenn Lightsey, E., and Leung, S., "A real-time kinematic GPS sensor for spacecraft relative navigation," *Aerospace Science and Technology*, Vol.6, No.6, October 2002, pp. 435-449.

[15] Kroes, R., and Montenbruck, O., "High Accuracy Kinematic Spacecraft Relative Positioning Using Dual-Frequency GPS Carrier Phase Data," *Proceedings of the 2004 National Technical Meeting of The Institute of Navigation*, San Diego, CA, January 2004, pp. 607-613.

[16] Hu, G., Abbey, D. A., Castleden, N., Featherstone, W. E., Earls, C., Ovstedal, O. and Weihing, D., "An approach for instantaneous ambiguity resolution for medium- to long-range multiple reference station networks," *GPS Solutions*, Vol. 9, No.1, April 2005, pp. 1-11.

[17] Parkins, A., "Increasing GNSS RTK availability with a new single-epoch batch partial ambiguity resolution algorithm," *GPS Solutions*, Vol. 15, No.4, October 2011, pp. 391-402.

[18] Farrell, J.A., *Aided navigation: GPS with high rate sensors*, McGraw-Hill, New York, 2008, Chaps. 5, 8.

[19] Montenbruck, O., and Kroes, R., "In-flight performance analysis of the CHAMP BlackJack GPS Receiver," *GPS Solutions*, Vol. 7, No.2, August 2003, pp. 74-86.

[20] Psiaki, M. L., and Mohiuddin, S., "Modeling, Analysis, and Simulation of GPS Carrier Phase for Spacecraft Relative Navigation," *Journal of Guidance, Control, and Dynamics,* Vol.30, No.6, November–December 2007, pp. 1628-1639.

[21] Montenbruck, O., and Ramos-Bosch, P., "Precision real-time navigation of LEO satellites using global positioning system measurements," *GPS Solutions*, Vol.12, No.3, July 2008, pp.187-198.

[22] Montenbruck, O., Kahle, R., D'Amico, S., and Ardaens, J.S., ''Navigation and Control of the TanDEM-X Formation," *Journal of the Astronautical Sciences*, Vol. 56, No. 3, September 2008, pp. 341–357.

[23] Tancredi, U., Renga, A., and Grassi, M., "Ionospheric path delay models for spaceborne GPS receivers flying in formation with large baselines", *Advances in Space Research*, Vol. 48, No. 3, August 2011, pp. 507–520.

[24] Lear, W. M., "GPS navigation for low-earth orbiting vehicles," NASA Lyndon B. Johnson Space Center, Mission planning and analysis division, 1st revision, NASA 87-FM-2, JSC-32,031, 1988.

[25] Montenbruck, O., Wermuth, M., Kahle, R, "GPS Based Relative Navigation for the TanDEM-X Mission - First Flight Results," *Proceedings of the 23rd International Technical Meeting of The Satellite Division of the Institute of Navigation* (ION GNSS 2010), Portland, OR, September 2010.

[26] Tancredi U., Renga, A., and Grassi, M., "Carrier-based Differential GPS for autonomous relative navigation in LEO," *AIAA Guidance, Navigation, and Control Conference*, Minneapolis, MN, August 2012.

[27] Tancredi U., Renga, A., and Grassi, M., "GPS-Based Relative Navigation of LEO Formations with Varying Baselines," *AIAA Guidance, Navigation, and Control Conference*, Toronto, Canada, August 2010.

[28] Teunissen, P.J.G., "The least-squares ambiguity decorrelation adjustment: a method for fast GPS integer ambiguity estimation," *Journal of Geodesy*, Vol.70, No.1-2, November 1995, pp. 65-82.

[29] Teunissen, P.J.G., and Verhagen, S., "GNSS ambiguity resolution: when and how to fix or not to fix," *VI Hotine-Marussi Symposium on Theoretical and Computational Geodesy*, International Association of Geodesy Symposia, Vol.132, 2008, pp 143-148.

[30] Verhagen, S., "The GNSS integer ambiguities: estimation and validation," Ph.D. Thesis, Delft University of Technology, The Netherlands, 2005.

[31] Teunissen, P.J.G., and Verhagen, S., "GNSS carrier phase ambiguity resolution: challenges and open problems," *Observing our Changing Earth Symposium*, International Association of Geodesy Symposia, Vol.133, 2008, pp 785-792.

[32] Melbourne, W.G., "The Case for Ranging in GPS-Based Geodetic Systems," *Proceedings of the First International Symposium on Precise Positioning with GPS*, Rockville, MD, April 1985, pp. 373–386.

[33] Wubbena, G.,"Software Developments for Geodetic Positioning with GPS Using TI 4100 Code and Carrier Measurements," *Proceedings of the First International Symposium on Precise Positioning with GPS*, Rockville, MD, April 1985, pp. pp. 403–412.

[34] Teunissen, P.J.G., "On the GPS widelane and its decorrelating property", *Journal of Geodesy*, Vol.71, No.9, August 1997, pp 577-587.

[35] Teunissen, P.J.G., Joosten, P, and Tiberius, C.C.J.M., "Geometry-free Ambiguity Success Rates in Case of Partial Fixing," Proceedings of the 1999 National Technical Meeting of The Institute of Navigation, San Diego, CA, January 1999, pp. 201-207.

[36] Kroes, R., "Precise Relative Positioning of Formation Flying Spacecraft using GPS," Ph.D. Thesis, Delft University of Technology, The Netherlands, 2006.

[37] Tapley B. D., Bettadpur S., Watkins M., and Reigber C., "The gravity recovery and climate experiment mission overview and early results," *Geophysical Research Letters,* Vol.31, No.9, May 2004, L09607.

[38] Davis G., Davis E., Luthcke S., and Hawkins K., ""Pre-Launch Testing of GPS Receivers for Geodetic Space Missions," Proceedings of the 13th International Technical Meeting of the Satellite Division of The Institute of Navigation (ION GPS 2000), Salt Lake City, UT, September 2000, pp. 2009-2018.

[39] Wu S.C., Kruizinga G., and Bertiger W, "Algorithm theoretical basis document for GRACE level 1B data processing," NASA Jet Propulsion Laboratory, revision 1.2, JPL D-27672, GRACE 327-741, 2006.